Journal of Materials Chemistry A

ROYAL SOCIETY OF CHEMISTRY

PERSPECTIVE

View Article Online
View Journal | View Issue

Check for updates

Cite this: J. Mater. Chem. A, 2025, 13, 37833

Si anodes for Li^+ batteries: what is the ideal structure?

Gregory Beaucage†‡*[a] and Siddharth V. Patwardhan ‡*[b]

Received 6th June 2025
Accepted 25th September 2025

DOI: 10.1039/d5ta04601g

rsc.li/materials-a

Significant research is focused on improving the performance of Li ion batteries (LIBs) by using Si in anodes due to its ten times higher theoretical capacity when compared with that of graphite, and it is also naturally abundant. However, there are many issues in using high Si content due to nearly threefold expansion of Si upon lithiation, leading to mechanical breakdown and loss of performance within a few cycles. This leads to the challenge of simultaneously optimising the stability, capacity, lithiation rates and solid electrolyte interphase (SEI) formation. It is unclear what the ideal porous structure is to meet the desired performance specifications. This perspective article proposes quantitative governing equations to correlate structural features with performance, which can provide guiding principles to design (meso) porous silicon (p-Si) structures. The structural features include nano-scale primary particles, and their meso-scale connectivity, degree of aggregation and tortuosity. We hypothesize that hierarchical aggregates of sub-micron networked particles will have an enhanced rate of lithiation yet with mechanical stability to withstand swelling *via* accordion expansion or disinterspersion (D.I.). Preliminary evaluation of these principles is presented, and future research avenues are outlined. To test these hypotheses, experimental investigations are needed to identify and compare various hierarchical structures that can maximise the criteria described above. These guiding principles will prove valuable for developing Si for LIB anodes, thereby accelerating their commercial uptake.

Open Access Article. Published on 27 October 2025. Downloaded on 6/20/2026 2:49:23 PM. This article is licensed under a Creative Commons Attribution 3.0 Unported Licence.

1. Background: introduction, issues and drivers

LIBs are currently the state-of-the-art battery cell type due to their high energy density and stability, making them widely preferred for energy storage. Post-lithium-ion-batteries (Na-ion batteries (SIBs), Li–S batteries (LSBs), solid-state batteries (SSBs) and Li–air batteries (LABs)) have an uncertain future due to issues associated with their performance and excessive investments required to establish their manufacturing, which is likely to outweigh the benefits.[1] Therefore, further research on cost reductions and increased energy density of LIBs is highly likely to provide the desired impact.

Graphite is the preferred anode for LIBs and makes up 48 mass percent of a cell and about 27% of the total EV battery pack making it the largest single component by mass.[2] However, an alternative is needed in order to meet growing demands such as higher energy density and lower costs while improving sustainability.[3,4] Furthermore, there have been recent issues pertaining to graphite availability and the supply chain, mainly driven by securing future access to meet the 8–10 times increase in the demands of energy storage using batteries.[5,6] Si provides 10 times higher theoretical capacity compared to graphite and is naturally abundant. Substitution of silicon for graphite could reduce the mass of anodes by a factor of 10 due to greater Li^+ specific capacity and higher cell potential. Silicon anode research has sought enhancement of specific capacity, lithiation/delithiation rates, and cycle life. As such, adding Si to graphite anodes has become common recently, with certain manufacturers using up to 10% Si. However, higher Si content is required to achieve the desired improvements. The increase in performance is complicated by up to a tripling of the silicon volume during the charging cycle,[7] which leads to decrepitation (Fig. 1 and 2) and formation of a new solid electrolyte interphase (SEI) which permanently depletes anode capacity. To accommodate silicon anodes in batteries, the volumetric breathing with charge cycles, associated with the greater specific capacity, must be included in the structural design.

Silicon also has a lower electrical conductivity (about 1/10 000) compared to graphite which reduces the charge/discharge rates. Further impacting the rates, the process of lithiation of silicon involves formation of an interstitial or a substitutional alloy which is slower than intercalation.[8] The formation of an

[a]Department of Chemical and Materials Engineering, University of Cincinnati, OH 45221, USA. E-mail: beaucag@ucmail.uc.edu

[b]Department of Chemical and Biological Engineering, University of Sheffield, Sheffield S1 3JD, UK. E-mail: s.patwardhan@sheffield.ac.uk

† Professor Gregory Beaucage sadly passed away in August 2025 while this manuscript was under revision.[60,61]

‡ The authors contributed equally.

Open Access Article. Published on 27 October 2025. Downloaded on 6/20/2026 2:49:23 PM.
This article is licensed under a Creative Commons Attribution 3.0 Unported Licence.

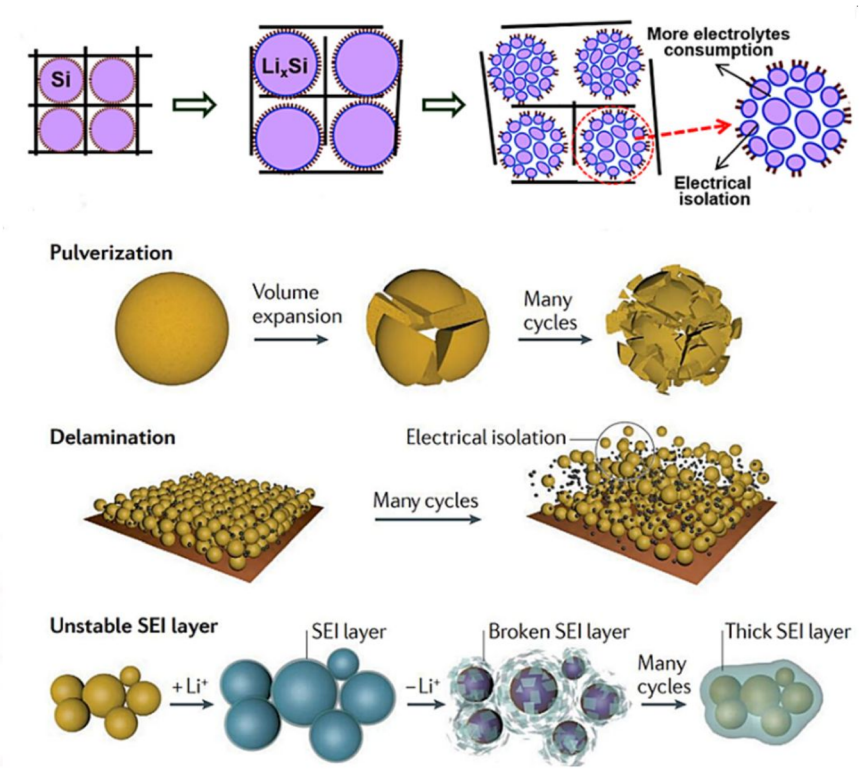

Fig. 1 Schematic representation of various mechanisms for decrepitation of silicon during lithiation. Image reproduced from ref. 9.

SEI that irreversibly consumes Li^+ provides a further barrier to transport of Li^+ and electrons. Decrepitation of silicon particles from cyclic swelling and contraction exacerbates the SEI problem leading to drastic capacity fade. Furthermore, the increase in Si loading in anodes is challenged by expensive manufacturing of anode-grade Si at the desired scale.[5]

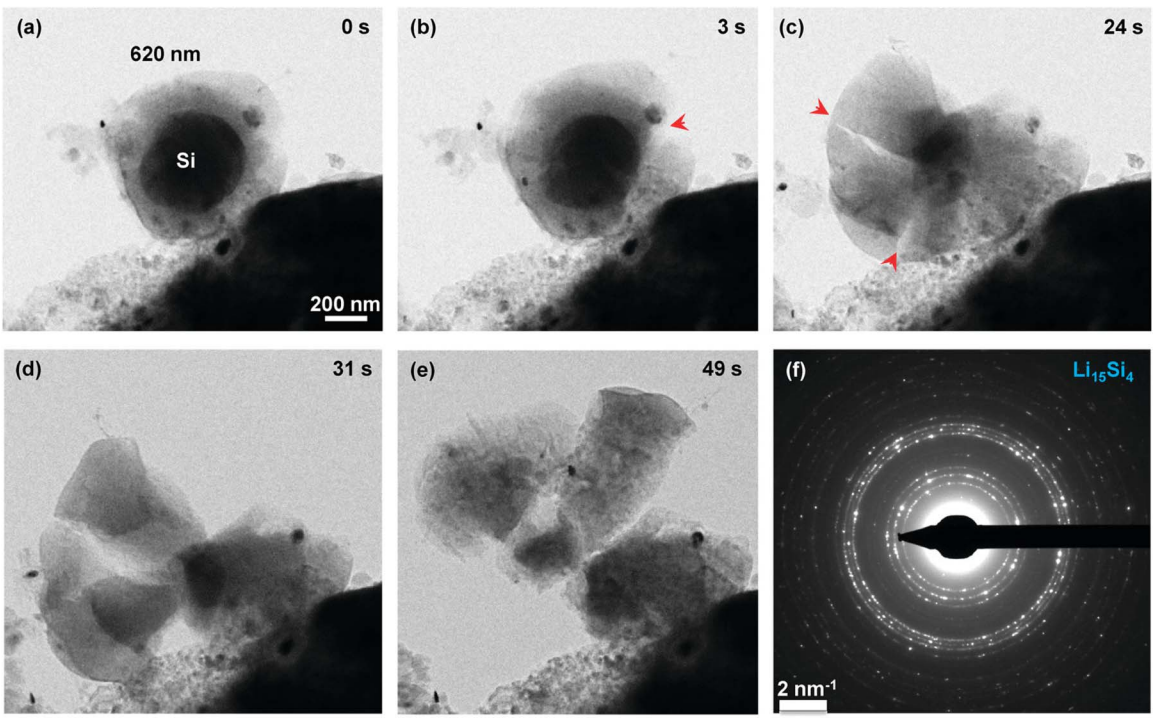

Fig. 2 (a–e) Lithiation of a 620 nm crystalline silicon particle with decrepitation. Red arrows indicate cracks. (f) Electron diffraction indicating the formation of polycrystalline $Li_{15}Si_4$ upon lithiation. Images reproduced from ref. 10.

 This journal is © The Royal Society of Chemistry 2025

Open Access Article. Published on 27 October 2025. Downloaded on 6/20/2026 2:49:23 PM.
This article is licensed under a Creative Commons Attribution 3.0 Unported Licence.

2. Addressing instability of Si

Research over the recent past has focused on addressing these challenges faced by Si, specifically, the mechanical instability during lithiation and delithiation cycles caused by the volumetric expansion. Many strategies are used to address the expansion-led loss of performance, and they can be categorised as follows (see Fig. 3):

- Engineering particle geometries (particle sizes, microstructure, crystallinity and morphology),
- Using Si-composites (including coatings and prelithiation),
- Developing formulations with suitable binders and electrolytes.

Generally, a common approach is to use sub-micron silicon particles such as reduced clay platelets, and rod structures with minor sizes smaller than the critical flaw size preventing breakage (decrepitation).[9,11–17] Some of the disadvantages to silicon as an anode material can be overcome through nanoparticles (NPs). There are a variety of ways reported in the literature to engineer particle structures (see Fig. 4 for examples). Particles smaller than the critical flaw size are not subject to cracking. High dilatational strains reduce the critical flaw size from microns to tens of nanometers.[18] Nanoparticles can more easily accommodate large volume changes arising from the formation of a swollen Li_xSi layer with the dilatational stress being alleviated at surfaces (see Fig. 5).[7] Diffusion distances are shorter for small particles, making lithiation/delithiation more rapid. The impact of low electrical conductivity is less limiting for shorter distances in nanoparticles embedded in a conductive matrix. Other strategies include creating carbon coatings or Si–C composites which can help mitigate issues arising from low conductivity of Si as well as SEI formation.

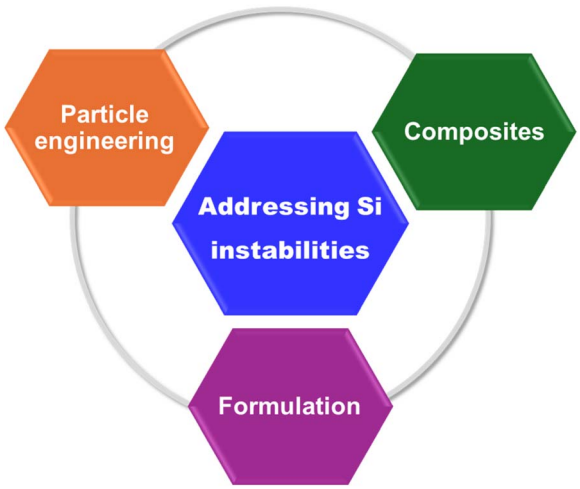

Fig. 3 A schematic showing three key strategies used for addressing the instabilities in Si-anodes.

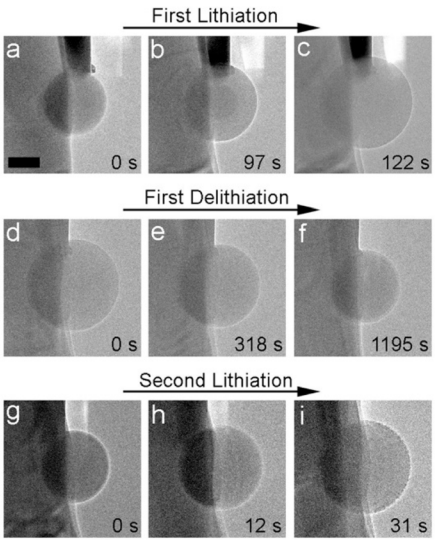

Fig. 5 Lithiation and delithiation of Si nanoparticles (the scale bar = 200 nm): first lithiation cycle (a–c), first delithiation (d–f), and second lithiation (g–i). Images reproduced from ref. 7.

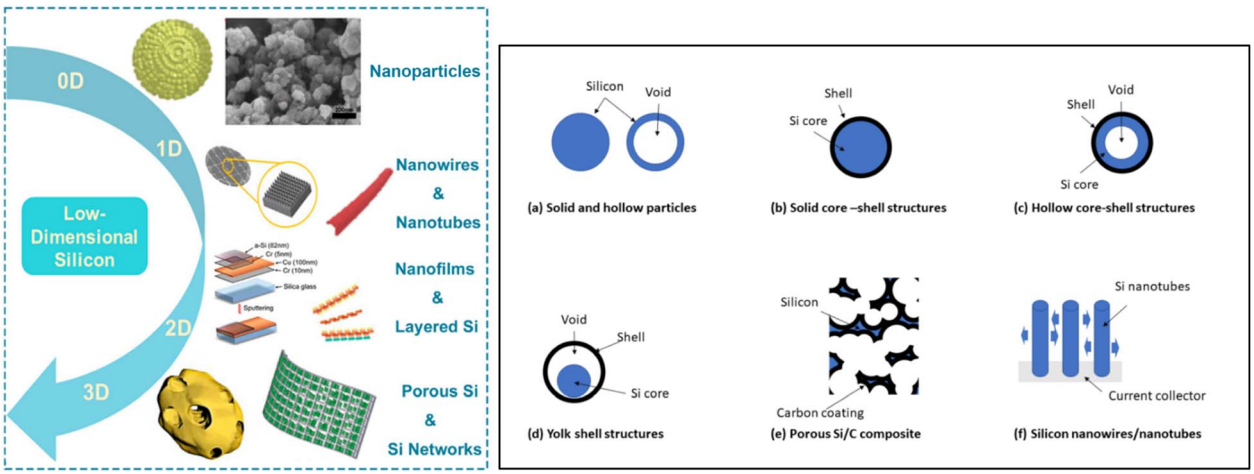

Fig. 4 Strategies to engineer the particle microstructure (left) and morphology to prevent breakage (decrepitation), right. Images reproduced from ref. 15 and 19.

Open Access Article. Published on 27 October 2025. Downloaded on 6/20/2026 2:49:23 PM. This article is licensed under a Creative Commons Attribution 3.0 Unported Licence.

Indeed, there is significant commercial interest in adopting these strategies for designing and developing high performance Si-based anodes. For example, Si deposited on porous carbons to produce Si–C composites are being developed, which are similar to the structures shown in part (e), right panel of Fig. 4.[20,21] Technologies for growing nanowires or micro-needles composed of pure silicon as well as Si–C composites have also been developed (such as those shown in part (f), right panel of Fig. 4).[22,23] There are also examples of depositing thin layers of Si on metals for direct use in anodes.[24]

Each of these strategies and combinations thereof has shown the potential to improve the performance of Si and can enable higher loading with graphite; however, 50% Si content and above in anodes is still not within our reach. This is because the strategies noted above provide only incremental improvements in Si performance. Manufacturing some of these complex structures can be very challenging, or at least they are economically prohibitive to manufacture due to multi-step, inefficient and slow processes. For example, Si NPs, while highly desirable for anodes, are notoriously uneconomical to manufacture and are not available on the market at scale.[19] Furthermore, there are issues with safety and sustainability of the methods producing desired Si structures. An overarching concern is that most developments have been focusing on one factor/feature (*e.g.* particle size or morphology or coating), instead of a holistic or an integrated approach which balances performance, scalability, costs and environmental factors.[25]

Nevertheless, these efforts have highlighted that the most promising structure is (meso)porous Si (p-Si). Experimental and simulation results have shown that porous structures at the nanoscale provide "breathing" space upon expansion during lithiation and hence improve the stability and performance.[26,27] This means that p-Si can be used at high Si content, thus overcoming the challenges outlined above, including economical and sustainable manufacture of such materials.[28] There are recent reports that such porous structures can be potentially manufactured.[23,29–31] As such, there have been many studies on the synthesis and testing of a range of p-Si structures; however, it is unclear what is the ideal porous structure which can simultaneously optimise multiple performance criteria. Guiding principles for designing high-performance Si-structures for LIB anodes are missing. This article aims to identify physics-based governing equations to help define "ideal" Si-structures.

3. Design principles for high-performance p-Si

It is hypothesized that the key performance criteria – capacity, stability (capacity retention), lithiation rates and solid electrolyte interphase (SEI) formation depend on hierarchical structural features of p-Si as follows:

(1) The SEI layer thickness is proportional to primary particle size;

(2) Lithiation/delithiation reaction rates are inversely proportional to the square of the primary particle size;

(3) Disinterspersion (accordion unfolding and folding) of Si aggregates depends on the hierarchical structure and mesoscale properties such as connectivity, the degree of aggregation and tortuosity;

(4) Specific capacity is dependent on the Si aggregate density and mass-fractal dimension.

Below we explain the rationale behind these relationships and their mathematical representations as governing equations.

3.1. Dependence of the SEI and lithiation rates on particle size

Capacity loss during charge cycles has been associated with the formation of an SEI layer which permanently removes lithium ions from the electrolyte. When the SEI layer cracks, with anode expansion and contraction, a new SEI layer forms, reducing the capacity of the cell even further. A thinner SEI layer is ideal, and it allows for more rapid ion transport. For macroscopic Si films, the SEI layer, after cycling, has been reported to be on the order of 100 nm, while for Si nanoparticles the SEI layer is on the order of 2–50 nm – there seems to be a correlation between the SEI layer thickness and nanoparticle size (eqn (1)).[15,32] As nanoparticle hydrostatic pressure is proportional to the inverse of nanoparticle (primary particle) size (d_p) from the Laplace equation (eqn (2)), or from simulations (500 to 20 000 atm pressure for a 20 nm silicon particle), and because the SEI layer formation involves a decrease in density which is opposed by hydrostatic pressure by Le Chatelier's principle, the SEI thickness depends directly on the primary particle size.[33] Therefore, the hypothesis is that smaller silicon particles should show better cycle retention due to more flexible, thin SEI layers.

$$t_{SEI} \propto d_p \tag{1}$$

$$P \propto 1/d_p \tag{2}$$

We note that as these particles form hierarchical structures, the exposed surface area will reduce depending on the aggregate structures and this may need to be accommodated within the proportionality constant of eqn (1). Furthermore, for lithiation, diffusion of Li from the electrolyte to Si particle surfaces is followed by diffusion and alloying within the Si particles. From Fig. 5, we know that alloying takes on the order of 10 to 100 seconds; hence, the alloying step is rate limiting and the diffusion time, τ^{Li^+}, depends on the diffusion distance in the particle (d_p^2), *i.e.* the lithiation rate (r_{Li^+}) increases as Si nanoparticles get smaller (eqn (3) and (4)).

$$\tau^{Li^+} \propto {d_p}^2 \tag{3}$$

$$r_{Li^+} \propto \frac{1}{{d_p}^2} \tag{4}$$

3.2. Dependence of disinterspersion on the aggregate structure

If one considers an interpenetrating network of branched aggregated silicon, p-Si, the structure has significant flexibility to volumetrically expand prior to subjecting the network to localized stress. This was demonstrated using chain mail as

 This journal is © The Royal Society of Chemistry 2025

Open Access Article. Published on 27 October 2025. Downloaded on 6/20/2026 2:49:23 PM.
This article is licensed under a Creative Commons Attribution 3.0 Unported Licence.

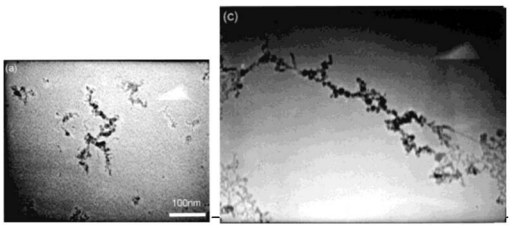

Fig. 6 Deformation of titania aggregates in TEM by >200% (from the image on left to the image on right). Image reproduced with permission from ref. 38.

a model for polymer networks,[34] which demonstrated that a volumetric expansion of 300% was possible with no local network stress. This expansion mechanism was termed disinterspersion and has been further demonstrated for aggregate materials[35] and experimentally observed in TEM images in Fig. 6.[36,37,39] The ability to disintersperse (expand) is low for a network of linear or highly branched aggregates and high when branching is low and the aggregates are convoluted.

Therefore, it is proposed that through the processes of disinterspersion (D.I.) and elastic expansion, networks of aggregated Si can accommodate large dilatational volume changes that occur during lithiation. The impact of meso- and micro-scale aggregate network structures on anode performance can be considered in relation to a fractal model where aggregates are ramified/branched clusters of primary particles as shown in Fig. 7.[40–42]

This disinterspersion (D.I.) or expansion can be linked to the structural features of a material if we consider the mass-fractal aggregate in Fig. 7. It shows a ramified mass-fractal aggregate such as p-Si, which can be described with an aggregate size R, a minimum or short circuit path p, and the primary particle size d_p. These parameters reflect the tortuosity, and a stick figure structure (lines) that reflects the topology, connectivity, or branching. Using these features, we define disinterspersion (D.I.) or the ability to expand as follows:

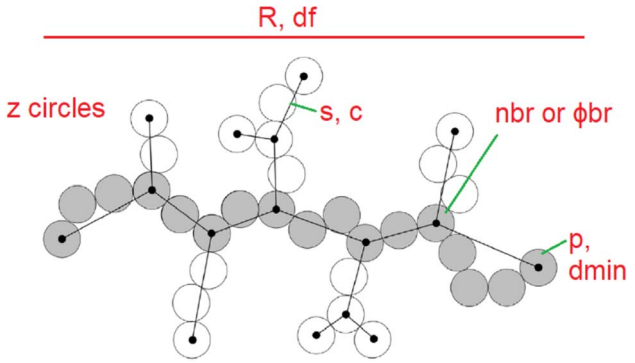

Fig. 7 2D schematic of an aggregate showing d_p = diameter of primary particles; R = end-to-end distance/aggregate size; c = connectivity (branching), $3 > c \geq 1$ for aggregates; d_{min} = tortuosity of aggregates independent of c, $3 > d_{min} \geq 1$; d_f = mass fractal dimension $d_f = c \times d_{min}$, $3 > d_f \geq 1$ reflecting packing density; z = degree of aggregation $=(R/d_p)^{d_f}$; p = minimum (short-circuit) path, grey circles $p = (R/d_p)^{d_{min}}$; s = connective path, black lines $s = (R/d_p)^c$.

$$\text{D.I.} \propto \frac{p \times d_p}{R} - 1 \tag{5}$$

Aggregates can be decomposed into a tortuous minimum path from which the aggregate attains elasticity, and a branched connective path which resists expansion due to interconnectivity. This is analogous to a knitted fabric with kinky fibers. The maximum meso-scale expansion occurs with a fully extended minimum path of length $p \times d_p$ from an original aggregate size R. For a linear structure that is not convoluted (primary particles connected in a straight line without any bends and hence without any possibility of expanding), $p \times d_p = R$ and disinterspersion (D.I.) = 0, that is, this aggregate structure (a rod) cannot expand through disinterspersion.

It is expected that a higher density aggregate would have a greater interspersion, but the topology (branching) might interfere with the ability to disintersperse or expand on swelling. A linear convoluted but unbranched structure, which can readily expand, will have a substructural minimum (or short-circuit) path, $p = (R/d_p)^{d_{min}}$ based on fractal theory,[40–43] where d_{min} is the minimum dimension that reflects the tortuosity of the aggregate independent of the connectivity, branching, or topology (c) such that the fractal dimension $d_f = c \times d_{min}$. Hence, substituting the definition of p in terms of R, d_p and d_{min}, in eqn (5), we get

$$\text{D.I.} \propto \left(\frac{R}{d_p}\right)^{(d_{min}-1)} - 1 \tag{6}$$

Furthermore, it is also known from fractal theory[40–43] that the degree of aggregation $z = (R/d_p)^{d_f}$ and that $d_f = c \times d_{min}$. Substituting z for R/d_p in eqn (6) and replacing d_f with d_{min}, we get

$$\text{D.I.} \propto z^{\left(\frac{1}{c}\right)\left(1-\frac{1}{d_{min}}\right)} - 1 \tag{7}$$

These parameters can be obtained from small-angle X-ray/neutron scattering and simulations, or can be approximated from micrographs.[40] Greater interspersion occurs when c is small (less branching) and d_{min} is large (more convoluted minimum paths). Topological connectivity interferes with the ability to disintersperse or expand on swelling. The structural model in Fig. 7 provides the framework[40] while the quantification of disinterspersion (eqn (7)) provides a new perspective. Therefore, the greatest degree of disinterspersion will be found for an unbranched aggregate, $c = 1$, that is fully convoluted to a 3D object ($d_{min} \to 3$, and $d_f \to 3$). However, such an aggregate would have no access for Li^+ to the primary particle surface. To maintain access to the surface, we desire a low value for c and a large value for d_{min}, but less than 3. It is therefore hypothesized that disinterspersion (D.I.) is encouraged when eqn (7) reaches a large value, which would be more than sufficient to accommodate meso- to micro-scale expansion of mass-fractal silicon aggregates during lithiation/delithiation. Eqn (7) indicates that D.I. has a minimum value of zero with no disinterspersion for any regular object (rod, disk, and sphere; for

Open Access Article. Published on 27 October 2025. Downloaded on 6/20/2026 2:49:23 PM. This article is licensed under a Creative Commons Attribution 3.0 Unported Licence.

instance for a linear structure $c = d_{min} = d_f = 1$). The maximum D.I. has a value of about $z^{2/3}$ for $c = 1$ and $d_{min} \rightarrow 3$. This can be a value much larger than the observed maximum volumetric expansion for silicon of 3 for full lithiation of silicon aggregates. Therefore, some p-silicon aggregates can demonstrate the ability to expand with little stress on the aggregate structure as quantified through the parameter D.I.

On the other hand, this new model also indicates that nanorod silicon or nano-platelet silicon (from clay) does not have the optimum topology/tortuosity for silicon anode materials that are subject to large volumetric expansion on lithiation; however, this needs to be tested. Isolated NPs, while individually can show better performance, possess poor connectivity in an electrode and will have a low density, leading to low specific capacity.[16,44,45] Alternatively, if they are closely packed, then there is no possibility of accessing the surface of the nanoparticles and they will not accommodate expansion and contraction.

3.3. Dependence of capacity on the aggregate structure

A second constraint on silicon anodes is to maximize the specific capacity by maximizing the packing density of silicon. This also maximizes the electrical connectivity of silicon nanoparticles. For mass-fractal aggregates, the density drops with increasing aggregate size as measured by z or R. Finally, access to the surface of the primary particles is necessary for lithiation/delithiation, so d_f must be smaller than 3 (for space filling, fully dense aggregates). Eqn (8) results in a larger density for larger d_f and smaller z, while eqn (7) results in larger D.I. with larger z leading to a potential optimization of the degree of aggregation, z. Both metrics, disinterspersion and density, improve with larger tortuosity, d_{min}.

$$\rho = \left(\frac{R}{D}\right)^{d_f-3} = z^{1-\frac{3}{d_f}} \quad (8)$$

In summary, it is proposed that aggregates of primary particles composing a network that satisfies the following three criteria can optimize anode performance:

(1) Thin SEI layers (minimize eqn (1)) and high transport rates (maximize eqn (4)),

(2) A high degree of interspersion (maximize eqn (7)), and.

(3) High density for high specific capacity, (maximize eqn (8)).

4. Implications of the governing equations

As a general rule of thumb, from eqn (1)–(8), we expect the smallest structures in a hierarchy to expand first, so it is most important for the smallest levels of the structure to display large interspersion in order to ensure capacity retention. From our hypothesis, the various hypothetical structures and their expected performance are shown in Fig. 8 and discussed below.

4.1. Aggregate structures and disinterspersion

Ramified Si nanoparticle aggregates, with the right balance of particle size, connectivity, degree of aggregation and tortuosity will provide high performance. It is proposed that this right balance requires (i) reducing primary particle size to minimize the SEI layer thickness and improve lithiation (fast charge rates), (ii) optimizing connectivity and tortuosity of hierarchical aggregates to allow disinterspersion (D.I.) or accordion folding to accommodate mesoscale breathing (swelling) of Si, and (iii) higher mass fractal dimensions for greater specific capacity. Based on these, four hypothetical structures are imagined and shown in Fig. 8 that are representative of materials typically produced and/or reported in the literature and can include colloidal, precipitated, sol–gel and pyrolytic silicas. The anticipated lithiation behaviour and energy storage performance of

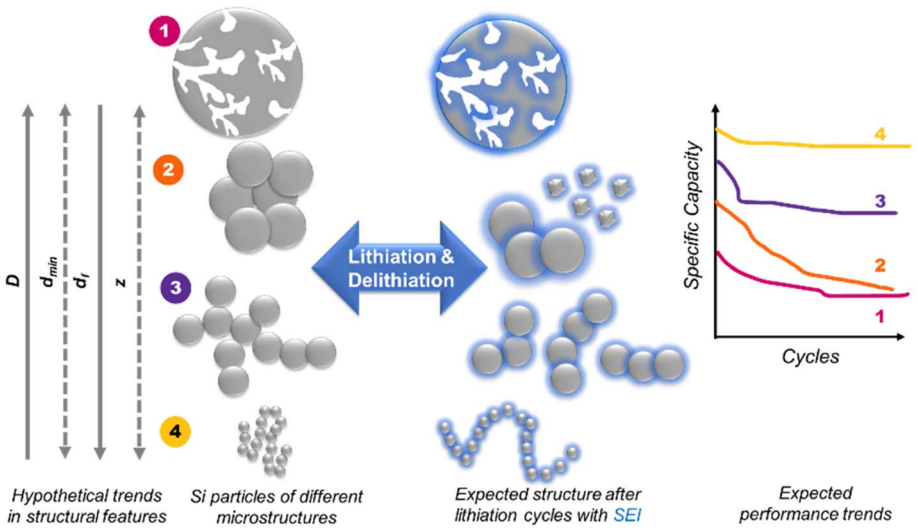

Fig. 8 A schematic showing a range of Si structures and their hypothetical performance; left delithiated and right lithiated (expanded). These are purely for hypothetical illustration where 1 = a porous structure, 2 = dense aggregates of large particles, 3 = branched network of small particles and 4 = an ideal structure. D is the parimary particle size.

 This journal is © The Royal Society of Chemistry 2025

Open Access Article. Published on 27 October 2025. Downloaded on 6/20/2026 2:49:23 PM.
This article is licensed under a Creative Commons Attribution 3.0 Unported Licence.

these hypothetical structures are also speculated on a qualitative basis using the hypothesis and design principles discussed above. Structure 1 shows a porous material with micro- and meso-pores (pores <50 nm). Material 2 represents dense aggregates of large particles, while structure 3 is a branched network of small particles. An ideal structure 4 is imagined composed of small primary particles, which would provide the highest D.I. Between structures 2, 3 and 4, we have shown different sizes and degrees of aggregation/densities. From the governing equations, structure 4 with the smallest primary particles and no branching is expected to outperform structure 3 with little larger particles and branching. Structure 2 is more compact with larger particles, and hence it is likely to perform worse than structures 3 and 4. Structure 1 is interesting with internal porosity and it is difficult to predict its performance, so the schematic is purely showing an illustration, to be confirmed with experimental results as discussed in Section 5.2. Similarly, these governing equations and hypothetical structures provide further basis to design future experimental research in order to build relations between this hypothesis and real-world or known materials. As an illustration, we applied these equations to a range of silica materials (commercial and academic), with varying aggregation levels, particle sizes and connectivity/branching, which were characterised in our previous work.[46] The materials included colloidal silica produced in lab using the well-known Stöber method, which represents nanoparticles with low levels of aggregation. Commercial Aerosil® silicas manufactured using the pyrolysis method were also included as they provide an example of branched structures composed of very small primary particles, while HiSil® precipitated silicas were included due to their dense aggregates of larger particles. Preliminary analysis of these materials using the governing equations indicated that some grades of precipitated silicas had a higher D.I. and a smaller SEI layer thickness, but their density and lithiation rates were not high enough. On the other hand, small colloidal particles and some of the pyrolytic silicas showed higher density; they are expected to form ticker SEI layers and not allow much expansion (low D.I.). This preliminary analysis is helpful in relating real-world materials and structures, and it provides practical insights. However, it is clear that a thorough experimental campaign is needed to either identify from existing structures the most ideal structures as per the governing equations or to explore synthetic methods to produce such materials. In addition, using this information for mapping the key structural features of Si materials with their synthetic method, processing parameters and electrochemical behaviours will be important as detailed in Section 5.2.

Based on the equations and the illustrations, we propose that ramified and hierarchical aggregates, that can be produced from various methods, form connected networks in composites,[47] which have significant ability to expand without subjecting the links of the branched network to significant stress due to a high degree of disinterspersion.[34] They are also known to display elasticity that can accommodate elastic strains greater than 300% (which is similar to the order of volumetric expansion upon full lithiation of Si) depending on the topology of the aggregates.[36,37,48–53] Friedlander demonstrated that ceramic and metallic aggregates display similar elasticity.[37,51–53] A similar process for solid aggregates in coal was also demonstrated[35] and more recently Müller demonstrated disinterspersion for rigid aggregate molecules.[39]

4.2. Feasibility of applying governing equations

Recently, mass-fractal aggregates of Si were used to study the effect of their particle size (not hierarchical structures) on their electrochemical performance.[54] Fig. 9a and b shows two types of particles used – Type I particles of about 200 nm in diameter with open fractal networks, and Type II particles of about 50 nm in diameter composed of dense 3D silicon clusters. These

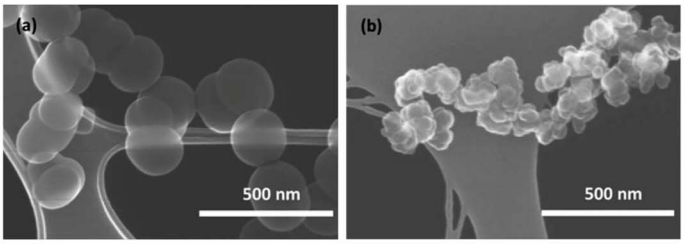

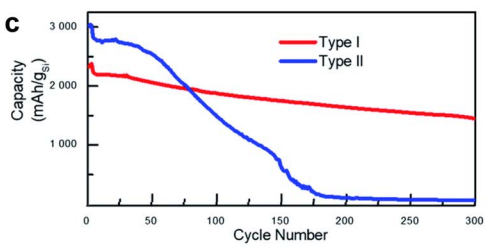

d

	Type I	Type II	Ratio
Initial Capacity, mAh/g	2350	3040	1.3
Initial Plateau, mAh/g	2200	2780	1.26
SEI Capacity Drop, mAh/g	144	266	1.85
Cycles for Initial Plateau	15	20	1.33
Final Cycles to 70%	300	80	3.75

Fig. 9 TEM micrographs of silicon particles showing (a) Type I and (b) Type II particles and (c) associated capacity *versus* cycle number.[54] (d) A summary of the capacity of batteries for type I and type II particles *versus* cycle number. First three cycles are at C/20, while the remaining are at C/10. Table shows values for some of the features in the plot.

Open Access Article. Published on 27 October 2025. Downloaded on 6/20/2026 2:49:23 PM.
This article is licensed under a Creative Commons Attribution 3.0 Unported Licence.

Table 1 Branched mass-fractal analysis of micrographs in Fig. 9a and b

	D, nm	z	P	R/D	d_f $\ln(z)/\ln(R/D)$	c $\ln(z)/\ln(p)$	d_{min}	d_f/c	$Sz^{(1/d_{min})}$	Disinterspersion $z^{(1/e)(1-1/d_{min}))}-1$	Density $z^{(1-3/d_f)}$	Rate of Li^+ diffusion $(1/D^2)/25 \times 10^{-6}$	SEI layer thickness $(D)/50$
Type I	200	28	17	8	1.60	1.18	1.36		11.5	1.11	0.054	1	4
Type II	50	253	70	20	1.85	1.30	1.42		49.5	2.52	0.031	16	1
Type III elemental	10	25	4	4	2.32	2.32	1		25	0	0.386	10 000	0.2

clustered particles form fractal networks. Using their TEM data, we have parameterized these aggregates (note: that study did not characterize the hierarchical structures of their materials; hence parameterization is crude). Our analysis of the micrographs (Table 1) shows that the degree of aggregation, z, is about an order of magnitude higher for Type II particles with a higher mass-fractal dimension, d_f.

Type II aggregates are more branched with a higher value for the connectivity dimension, c. The minimum path through the aggregates is more convoluted in Type II particles (a higher d_{min}). Using these structural features and applying the governing equations, it is likely that Type I particles will display good capacity retention at a high specific capacity. With lithiation cycles, Type II particles, which have a much higher degree of aggregation, should swell progressively with each new cycle, exposing more accessible surface for lithiation/SEI formation, eventually breaking the clusters apart. Fig. 9c shows the specific capacity change with cycle number for the aggregates (see summary in Fig. 9d). The first three cycles are at C/20 to aid the formation of the initial SEI layer which results in a capacity drop in both cases. The remaining cycles are at C/10. Type II particles have a greater initial specific capacity due to improved access to Si in the smaller primary particle size and high packing density and a greater drop in SEI formation followed by a plateau at a higher capacity. After the first 20–40 cycles, Type II particles show a rapid decline in capacity, potentially due to the primary particle clusters breaking apart and forming new SEI materials, which eventually leads to the observed drastic drop in specific capacity. While there is some matching between the estimated structural features and the observed electrochemical performance, it is not possible to fully predict the behavior due to lack of full structural information of these particles. As such, a detailed and reliable prediction of performance would require *in operando* measurements and X-ray scattering measurements which can directly determine the 3D structural parameters.[40]

5. Conclusions and outlook

5.1. Conclusions

Given the increase in the demand for batteries and the drive towards higher performance, the use of greater fractions of Si in anodes is required due to its nearly ten-fold higher capacity when compared with graphite. However, upon lithiation, Si expansion to ~300% leads to breakage and loss in performance. Many strategies are used to address this issue, and while many of them face issues with scale-up and economics, using porous Si seems viable both from performance and manufacturing perspectives. Despite this progress, design criteria for high-performance porous structures are unknown and progress has been mis-directed. In this article, we presented new quantitative governing equations that are developed using fundamental physical rules to allow a comparison and better design of Si structures. Such a combination of structural features would lead to a dense network of weakly branched nanoaggregates in a conductive matrix. Hence, it is anticipated that engineered mass fractal aggregates composed of nanoparticles would be useful for accommodating dilatometric expansion and

This journal is © The Royal Society of Chemistry 2025

Open Access Article. Published on 27 October 2025. Downloaded on 6/20/2026 2:49:23 PM.
This article is licensed under a Creative Commons Attribution 3.0 Unported Licence.

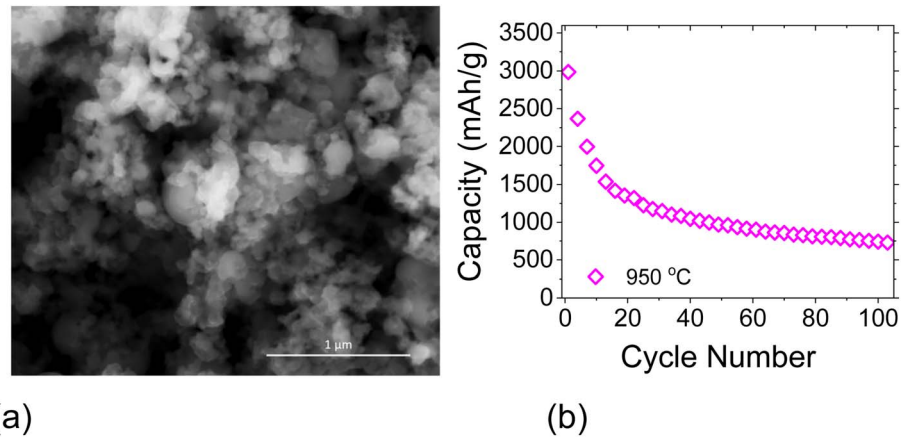

Fig. 10 Bioinspired silica, reduced at 950 °C; (a) SEM micrograph and (b) capacity *versus* cycle number, image reproduced with permission from ref. 27.

contraction of silicon, while also providing a high specific capacity and lithiation rate. The size of primary particles in the aggregates will be well below the critical flaw size and they have extensive accessible surface area which will allow rapid diffusion of lithium ions for lithiation and delithiation over the short distances in the nanoparticles. On the meso- to macro-scale, networks of tortuous aggregates (and associated porosity) can accommodate this dilatational breathing in lithiation cycles through elastic deformation and disinterspersion. Preliminary analysis of available literature suggests that these design principles are highly likely to provide a strong basis for designing optimal Si structures. These can be tested by selecting a range of Si structures.

5.2. Outlook

To test the hypotheses detailed above, a range of silicon structures should be investigated experimentally. The ideal design of Si-structures is defined above; however, such structures are not yet reported in the literature. Hence, finding a method to produce such structures is desirable. Metallothermic reduction (MTR) is a shape-preserving method to convert silica and silicates to silicon and has the potential to make the desired networks of aggregated Si structures.[26,27,55] Furthermore, MTR has been shown to be a scalable, sustainable and economical method that is ideally suitable for commercial production of anode-grade Si.[28,29,56] In addition, well defined Si nanoparticles of varying sizes can be used for comparison. Such particles can be produced using either chemical vapor deposition or pyrolysis of silane gas.[54]

In our previous work,[27] we produced Si nanoaggregates by MTR at 950 °C using silica aggregates. The particles have a bimodal population, composed of smaller (14 nm) and larger particles (170 nm), as shown in Fig. 10a. The small particles are likely to show a low interspersion and high density, d_f, and connectivity, c, which means that they are topologically unable to structurally expand without breaking. The larger particles show high interspersion and can structurally expand, but low density/capacity. This implies that this material will have high initial capacity arising from the high density of smaller particles, but it would rapidly reduce due to their low interspersion. Subsequent cycling is likely to maintain the (low) capacity, mainly due to the larger particles withstanding the expansion but their low density results in lower capacity. Fig. 10b shows the capacity over 100 cycles, which fully matches the predictions. This closely follows the governing equations, which suggests that capacity retention correlates with interspersion and density, while capacity is related to particle size. Furthermore, this also provides confirmation that MTR is a promising method to produce desired Si structures, with a good control over properties.

If we are able to use mass-produced commercial silica or custom silica with the desired structure, then MTR can produce the right types of Si that are suitable for high-performance in LIB anodes. Mass-fractal silica aggregates are often formed by solution (precipitated, colloidal, or silica gel) or flame (fumed) synthesis. Silica can also be produced using base catalysts leading to larger spherical and close to monodisperse particulate aggregates or independent silica spheres by the Stöber process. Fumed silica has extremely small silica primary particles and a typically high degree of aggregation while solution silica generally displays larger primary particle size and a lower degree of aggregation. A range of silica aggregate structures are possible with primary particle sizes from 1 nm to several microns and the degree of aggregation ranging from 1 to about 2000 with variable topologies (branch content and tortuosity).[46]

Future research should focus on two key aspects. Firstly, identifying and comparing methods to produce various hierarchical structures that maximise the criteria described above is important. While MTR is one such promising method, there are likely others too such as chemical vapor deposition and pyrolysis of silane gas, especially for producing controlled nanoparticles of desired sizes.[54] A holistic comparison of these structures and methods of their production should be made on the basis of their multi-criteria performance metrics, scalability/manufacturability, environmental impact and economics.[25] Considering a single criterion or not using an integrated

Open Access Article. Published on 27 October 2025. Downloaded on 6/20/2026 2:49:23 PM. This article is licensed under a Creative Commons Attribution 3.0 Unported Licence.

approach can lead to unsurmountable hurdles in developing and commercialising promising technologies.[57,58] Secondly, in-depth studies are required to understand the structural hierarchy in Si anodes and their performance. Developing links between processing, hierarchical structures and electrochemical performance will help create fundamental design criteria to improve performance. Specifically, a systematic mapping of structural features during the formation of such Si structures and *in operando* measurements of electrochemical performance is crucial. Examples include the use of a combination of *in situ* and *in operando* SAXS and diffraction to study the structures and their lithiation/delithiation, complemented by electron microscopy, spectroscopy and electrochemical testing. SAXS and USAXS can resolve the average structural features over thousands of nanoparticles on a second time scale. This information can be coupled with electrochemical measurements to understand the hierarchical structural basis for anode performance. It has been observed that during the charging/discharging cycles, isolated Si nanoparticles can aggregate and hence the performance changes dynamically. While the governing equations would not change in principle, the inputs based on the characteristics of the Si structures will change dynamically. A combination of *in situ* and *in operando* measurements discussed above would be valuable in investigating performance variations as a result of dynamic changes to the Si structure during cycling. Furthermore, Pair Distribution Function (PDF) analysis by X-ray diffraction provides information on chemical bonds (and speciation) from both the crystalline and amorphous components and hence is a powerful tool for *in operando* measurement of electrochemical processes in LIBs. While *in operando* PDF is yet to be used over lithiation cycles for hierarchical aggregates of Si, a study published recently on 100 nm Si NPs (not hierarchical aggregates) investigated just one cycle.[59] This first *in operando* study demonstrates that such measurements are possible and contain important kinetic and mechanistic information concerning the lithiation process.

Conflicts of interest

SVP is a co-founder of a spin-out company, AmpliSi Ltd, that will be producing silicon for LIBs.

Data availability

No primary research results, software or code have been included and no new data were generated or analysed as part of this perspective.

Acknowledgements

We are thankful for financial support for this work from the Faraday Institution (Seed Project FIRG041 and Industry Sprint FIRG068), the Innovation Launchpad Network+ Researchers in Residence Scheme (RIR16G221130-1), the University of Cincinnati International Strategic Partner Incentive Grant and the Fulbright Scholar Award.

References

1 F. Duffner, N. Kronemeyer, J. Tübke, J. Leker, M. Winter and R. Schmuch, *Nat. Energy*, 2021, **6**, 123–134.
2 E. White, *Here's Why Graphite Is Needed for Affordable Electric Vehicles*, Autoweek, 2023.
3 F. Degen, M. Winter, D. Bendig and J. Tübke, *Nat. Energy*, 2023, **8**, 1284–1295.
4 *Silicon battery Market to Surge at a Robust Pace in Terms of Revenue Over 2022-2030*, 2022, **https://www.digitaljournal.com**.
5 *Graphite Shortage: Supply Chain Strategies for EV Makers*, 2023, **https://www.gep.com/blog/mind/graphite-shortage-supply-chain-strategies-for-ev-makers**.
6 E. White, W. Langley and H. Dempsey, 2023, **https://www.ft.com/content/8af8c05c-8e54-40e9-9051-5a0b2b036c32**.
7 M. T. McDowell, S. W. Lee, J. T. Harris, B. A. Korgel, C. Wang, W. D. Nix and Y. Cui, *Nano Lett.*, 2013, **13**, 758–764.
8 W. Wan, Q. Zhang, Y. Cui and E. Wang, *J. Phys.: Condens. Matter*, 2010, **22**, 415501.
9 X. Xia, X. Qian, C. Chen, W. Li, D. He, G. He and H. Chen, *J. Energy Storage*, 2023, **72**, 108715.
10 X. H. Liu, L. Zhong, S. Huang, S. X. Mao, T. Zhu and J. Y. Huang, *ACS Nano*, 2012, **6**, 1522–1531.
11 M. Ashuri, Q. He and L. L. Shaw, *Nanoscale*, 2016, **8**, 74–103.
12 P. Li, G. Zhao, X. Zheng, X. Xu, C. Yao, W. Sun and S. X. Dou, *Energy Storage Mater.*, 2018, **15**, 422–446.
13 Z. Zhao, F. Chen, J. Han, D. Kong, S. Pan, J. Xiao, S. Wu and Q.-H. Yang, *Adv. Energy Mater.*, 2023, **13**, 2300367.
14 M. Ge, C. Cao, G. M. Biesold, C. D. Sewell, S.-M. Hao, J. Huang, W. Zhang, Y. Lai and Z. Lin, *Adv. Mater.*, 2021, **33**, 2004577.
15 Y. Li, Q. Li, J. Chai, Y. Wang, J. Du, Z. Chen, Y. Rui, L. Jiang and B. Tang, *ACS Mater. Lett.*, 2023, **5**, 2948–2970.
16 Z. Cheng, H. Jiang, X. Zhang, F. Cheng, M. Wu and H. Zhang, *Adv. Funct. Mater.*, 2023, **33**, 2301109.
17 A. A. AbdelHamid, A. Mendoza-Garcia and J. Y. Ying, *Nano Energy*, 2022, **93**, 106860.
18 R. A. Huggins and W. D. Nix, *Ionics*, 2000, **6**, 57–63.
19 *Silicon as anode material: Is it "the next big thing"?*, 2023. **https://futurebatterylab.com/silicon-as-anode-material-is-it-the-next-big-thing/**.
20 H. R. Costantino, A. Dhanabalan, A. J. Sakshaug, C. Timmons and R. Patel, *US Pat.*, US20220246914A1, 2022.
21 G. Yushin, O. Magazynskyy, P. Dixon and B. Hertzberg, *US Pat.*, US11515528B2, 2022.
22 Y. Pan, X. Duan, R. S. Dubrow, J. L. Goldman, S. Mostarshed, C. Niu, L. T. Romano and D. Stumbo, *US Pat.*, US7105428B2, 2006.
23 L. Canham, C. M. Friend, W. J. Macklin and S. Brown, *US Pat.*, US10090513B2, 2013.
24 A. P. Didden, *US Pat.*, US20220328814A1, 2020.
25 R. Pilling, S. R. Coles, M. R. Knecht and S. V. Patwardhan, *Commun. Eng.*, 2023, **2**, 78.

 This journal is © The Royal Society of Chemistry 2025

Open Access Article. Published on 27 October 2025. Downloaded on 6/20/2026 2:49:23 PM. This article is licensed under a Creative Commons Attribution 3.0 Unported Licence.

26 J. Entwistle, A. Rennie and S. Patwardhan, *J. Mater. Chem. A*, 2018, **6**, 18344–18356.
27 J. E. Entwistle, G. Beaucage and S. V. Patwardhan, *J. Mater. Chem. A*, 2020, **8**, 4938–4949.
28 M. Yan, S. Martell, M. Dasog, S. Brown and S. V. Patwardhan, *J. Power Sources*, 2023, **588**, 233720.
29 J. E. Entwistle and S. V. Patwardhan, *RSC Adv.*, 2021, **11**, 3801–3807.
30 Z. Chen and Y. Zhang, WO2022046943A1, 2021.
31 I. Dutta, B. A. Kent, P. D. Tepesch, S. M. O'Malley and R. E. Youngman, *US Pat.*, US11139473B2, 2020.
32 M. Nie, D. P. Abraham, Y. Chen, A. Bose and B. L. Lucht, *J. Phys. Chem. C*, 2013, **117**, 13403–13412.
33 T. Hawa and M. R. Zachariah, *J. Chem. Phys.*, 2004, **121**, 9043–9049.
34 J. Bastide, C. Picot and S. Candau, *J. Macromol. Sci. B*, 1981, **19**, 13–34.
35 P. C. Painter, J. Graf and M. M. Coleman, *Energy Fuels*, 1990, **4**, 393–397.
36 S. K. Friedlander, H. D. Jang and K. H. Ryu, *Appl. Phys. Lett.*, 1998, **72**, 173–175.
37 S. K. Friedlander, K. Ogawa and M. Ullmann, *Powder Technol.*, 2001, **118**, 90–96.
38 Y. J. Suh, M. Ullmann, S. K. Friedlander and K. Y. Park, *J. Phys. Chem. B*, 2001, **105**, 11796–11799.
39 T. Müller, J.-U. Sommer and M. Lang, *Macromolecules*, 2021, **54**, 4601–4614.
40 G. Beaucage, *Phys. Rev. E*, 2004, **70**, 031401.
41 G. Beaucage, H. K. Kammler and S. E. Pratsinis, *J. Appl. Crystallogr.*, 2004, **37**, 523–535.
42 G. Beaucage and D. W. Schaefer, *J. Non-Cryst. Solids*, 1994, **172–174**, 797–805.
43 G. Beaucage, *J. Appl. Crystallogr.*, 1996, **29**, 134–146.
44 T. Yoon, C. C. Nguyen, D. M. Seo and B. L. Lucht, *J. Electrochem. Soc.*, 2015, **162**, A2325.
45 L. Sun, Y. Liu, L. Wang and Z. Jin, *Adv. Funct. Mater.*, 2024, **34**, 2403032.
46 A. Mulderig, G. Beaucage, K. Vogtt, H. Jiang and V. Kuppa, *J. Aerosol Sci.*, 2017, **109**, 28–37.
47 L. Song, Z. Wang, X. Tang, L. Chen, P. Chen, Q. Yuan and L. Li, *Macromolecules*, 2017, **50**, 7249–7257.
48 Y. J. Suh, S. V. Prikhodko and S. K. Friedlander, Manipulations of nanoparticle chain aggregates in transmission electron microscopy, in *Symposium on Nanostructured Interfaces held at the 2002 MRS Spring Meeting*, San Francisco, California, 2002, pp. 81–86.
49 W. Z. Rong, W. Q. Ding, L. Mädler, R. S. Ruoff and S. K. Friedlander, *Nano Lett.*, 2006, **6**, 2646–2655.
50 R. Bandyopadhyaya, W. Z. Rong and S. K. Friedlander, *Chem. Mater.*, 2004, **16**, 3147–3154.
51 W. Rong, A. E. Pelling, A. Ryan, J. K. Gimzewski and S. K. Friedlander, *Nano Lett.*, 2004, **4**, 2287–2292.
52 Y. J. Suh and S. K. Friedlander, *J. Appl. Phys.*, 2003, **93**, 3515–3523.
53 K. Ogawa, T. Vogt, M. Ullmann, S. Johnson and S. K. Friedlander, *J. Appl. Phys.*, 2000, **87**, 63–73.
54 S. Y. Lai, J. P. Mæhlen, T. J. Preston, M. O. Skare, M. U. Nagell, A. Ulvestad, D. Lemordant and A. Y. Koposov, *Nanoscale Adv.*, 2020, **2**, 5335–5342.
55 Z. Bao, M. R. Weatherspoon, S. Shian, Y. Cai, P. D. Graham, S. M. Allan, G. Ahmad, M. B. Dickerson, B. C. Church, Z. Kang, H. W. Abernathy Iii, C. J. Summers, M. Liu and K. H. Sandhage, *Nature*, 2007, **446**, 172–175.
56 M. Yan and S. V. Patwardhan, *RSC Adv.*, 2021, **11**, 35182–35186.
57 R. Pilling and S. V. Patwardhan, *ACS Sustain. Chem. Eng.*, 2022, **10**, 12048–12064.
58 J. Siota, *Linked Innovation*, Palgrave Macmillan Cham, 2018.
59 D. S. Wragg, C. Skautvedt, A. Brennhagen, C. Geiß, S. Checchia and A. Y. Koposov, *J. Phys. Chem. C*, 2023, **127**, 23149–23155.
60 A. Rao, *In Memoriam: Gregory Beaucage, Chemical engineering professor was known for his polymer research and industry partnerships*, **https://www.uc.edu/news/articles/2025/09/in-memoriam–gregory-beaucage-phd.html**, accessed 16/9/2025.
61 G. Beaucage, 2025, **https://www.memorialfuneralhome.com/obituaries/gregory-beaucage**, accessed 16/9/2025.